JACS
JOURNAL OF THE AMERICAN CHEMICAL SOCIETY

ARTICLE

pubs.acs.org/JACS

Topological and Electronic Influences on Magnetic Exchange Coupling in Fe(III) Ethynylbenzene Dendritic Building Blocks

Wesley A. Hoffert,† Anthony K. Rappé, and Matthew P. Shores*

Department of Chemistry, Colorado State University, Fort Collins, Colorado 80523-1872, United States

Supporting Information

ABSTRACT: Significant variance in the magnitude of reported exchange coupling parameters (both experimental and computed) for paramagnetic transition metal−ethynylbenzene complexes suggests that nuances of the magnetostructural relationship in this class of compounds remain to be understood and controlled, toward maximizing the stability of high-spin ground states. We report the preparation, electrochemical behavior, magnetic properties, and results of computational investigations of a series of iron ethynylbenzene complexes with coordination environments suitable for metallodendrimer assembly: $[(dmpe)_2FeCl(C_2Ph)](OTf)$ (**1**), $[(dmpe)_4Fe_2Cl_2(\mu\text{-}p\text{-}DEB)](BAr^F{}_4)_2$ (**2**), $[(dmpe)_6Fe_3Cl_3(TEB)]$ (**3**), $[(dmpe)_6Fe_3Cl_3(\mu_3\text{-}TEB)](OTf)_3$ (**4**), and $[(dmpe)_4Fe_2Cl_2(\mu\text{-}m\text{-}DEB)](BAr^F{}_4)_2$ (**5**) [dmpe = 1,2-bis(dimethylphosphino)ethane; *p*-H_2DEB = 1,4-diethynylbenzene; $BAr^F{}_4$ = tetrakis[3,5-bis(trifluoromethyl)phenyl]borate; H_3TEB = 1,3,5-triethynylbenzene; *m*-H_2DEB = 1,3-diethynylbenzene]. As expected, the ligand topology drives the antiferromagnetic coupling in **2** ($J = -134$ cm^{-1} using the $\hat{H} = -2J\hat{\mathbf{S}}_1 \cdot \hat{\mathbf{S}}_2$ convention) and the ferromagnetic coupling in **4** and **5** ($J = +37$ cm^{-1}, $J' = +5$ cm^{-1} for **4**; $J = +11$ cm^{-1} for **5**); the coupling is comparable to but deviates significantly from values reported for related Cp*-containing species (Cp* = η^5-C_5Me_5). The origins of these differences are explored computationally: a density functional theory (DFT) approach for treating the coupling of three spin centers as a linear combination of single-determinantal descriptions is developed and described, and the results of these computations can be generalized to other paramagnetic systems. Unrestricted B3LYP hybrid DFT calculations performed on rotamers of **4** and **5** and related complexes, as well as Cp* analogues, provide *J* values that correlate with the experimental values. We find that geometric considerations dominate the magnetism of the Cp* complexes, while topology and alkynyl ligand electronics combine more subtly to drive the magnetism of the new complexes reported here. These calculations imply that substantial magnetic exchange parameters, with accompanying well-isolated high-spin ground states, are achievable for ethynylbenzene-bridged paramagnetic metallodendrimers.

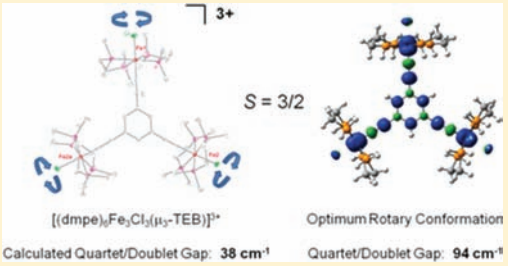

INTRODUCTION

In search of increased processor speeds, larger data storage densities, and improved material and energy efficiencies, recent efforts have focused on the control of charge and/or spin at the molecular level. Employing carbon-rich ligands as bridges for metal ion species represents a promising route in that the ligands are tunable by well-established synthetic methods and often display good orbital and energetic overlap with the metal ends. Especially relevant to technological applications are polyyne ligands bridging redox-active metal centers: they have been shown to be exceptional conduits for electricity at the nanoscale, and this discovery in turn has energized the relatively new field of molecular electronics.[1,2]

Enhancing intramolecular communication is also vital to the development of nanoscale magnets. Research in single-molecule magnet (SMM) clusters has progressed from the discovery of slow magnetic relaxation in a $Mn_{12}O_{12}$ molecule[3] to the isolation of hundreds of molecular species that show similar properties,[4,5] including a recent report of magnetic hysteresis in a dinuclear terbium complex at a record-high temperature of 14 K.[6] The origin of this phenomenon is rooted in the combination of a high-spin ground state (S) and a negative molecular easy-axis magnetic anisotropy (D), as defined in eq 1:

$$\hat{H} = D\hat{S}_z^2 + E(\hat{S}_x^2 + \hat{S}_y^2) \quad (1)$$

Importantly, for species where exchange interactions dominate, the coupling constants (J) must be maximized in order to avoid populating lower-spin excited states. In this regard, rigid, highly conjugated bridging ligands might be anticipated to generate robust magnetic coupling over long distances as a result of tailor-made orbital communication pathways.[7] We note that SMM behavior was recently observed for the first time in mono- and dinuclear organometallic lanthanide complexes,[8,9] but to our knowledge, only one SMM where magnetic communication occurs through a noncyanide carbon linkage is known.[10]

Here, arylalkynyl ligands based on 1,3,5-triethynylbenzene (H_3TEB) avail themselves as potential candidates for generating strong magnetic exchange coupling and perhaps negative zero-field splitting parameters.[11−13] The deprotonated congeners

Received: July 26, 2011
Published: November 08, 2011

have been employed as bridging ligands in second- and third-row transition-metal metallodendrimers because of their rigidity and amenability to a regular spatial arrangement of many diamagnetic transition metals around a C_6H_3 core.[14−17] Although some paramagnetic ethynylbenzene-bridged complexes are known, the reported coordination environments of the metal ions are not suitable for elaboration to larger assemblies. It has been shown that these ligands may permit significant spin communication between transition-metal centers, but the strength of the coupling appears to be dependent on subtle and not well understood factors. Lapinte and co-workers synthesized an impressive array of paramagnetic [(dppe)(Cp*)Fe^{III}]-containing complexes [dppe =1,2-bis(diphenylphosphino)ethane; Cp* = η^5-C_5Me_5) with various acetylide connecting ligands in order to study their magnetic and charge-transfer properties.[18−24] The exchange coupling constants extracted for the triferric complex [(dppe)$_3$(Cp*)$_3$$Fe^{III}_3$(TEB)](PF$_6$)$_3$ are relatively small at 9.6 and 4.4 cm^{-1} (using the $\hat{H} = -2J\hat{\mathbf{S}}_1 \cdot \hat{\mathbf{S}}_2$ convention).[19] Meanwhile, in regard to related *m*-diethynylbenzene-bridged dinuclear complexes, the ferromagnetic coupling for [(dppe)$_2$(Cp*)$_2$$Fe^{III}_2$(*m*-DEB)](PF$_6$)$_2$ (*m*-H_2DEB = 1,3-diethynylbenzene) was found to be significantly stronger (J = 65 cm^{-1}); a recent reinvestigation by Paul and co-workers found that the triplet ground state is fully populated at 300 K, implying a ferromagnetic exchange strength of at least 150 cm^{-1}.[25] Differences in the reported magnetic exchange coupling values have been attributed to impurities[18,26] and to varying coordination geometries and relative orientations of spin-containing orbitals.[27,28]

Relevant to the incorporation of first-row transition metals into ethynylbenzene-based dendrimers, Field and others prepared Fe^{II} and Fe^{III} σ-acetylide complexes with a $(P_4)(\sigma\text{-}C)(Cl)$ first coordination sphere and studied their electrochemical and intervalence charge-transfer properties.[29−32] Since these types of species contain the necessary coordination geometry for stepwise ligand substitution, an examination of the magnetic properties for the individual "building blocks" is needed for the properties of larger assemblies to be more easily understood. Berben has found that *trans,trans*-[(dmpe)$_4$$Fe_2$$Cl_2$(*m*-DEB)](PF$_6$)$_2$ [dmpe =1,2-bis(dimethylphosphino)ethane] is consistent with a coupling constant of 41 cm^{-1}, a value that is in line with Lapinte's earliest report on the Cp* analogue.[33] All of these results suggest that under certain circumstances, strong magnetic coupling may be produced by alkynylbenzene bridging ligands, provided that robust magnetostructural correlations can be established.

In view of the variance found in the magnetic and theoretical treatments applied to a relatively small number of ethynylbenzene-bridged complexes, a systematic study of the factors involved in magnetic exchange is warranted. Herein we present the syntheses, magnetic characterizations, and results of computational investigations of a family of di- and trinuclear complexes containing [(dmpe)$_2$$Fe^{III}$Cl] units connected by DEB^{2-} and TEB^{3-} bridging ligands. We compare magnetic data obtained on the new complexes with those for the previously reported, structurally similar species. We describe a novel density functional theory (DFT) approach for treating the coupling of three spin centers as a linear combination of single-determinantal descriptions and place all of the complexes in the same computational framework, allowing subtle differences in the geometries and electronic structures of the complexes to be related to the observed magnetic properties; the results of these computations can be generalized to other paramagnetic systems. We find that [(dmpe)$_2$$Fe^{III}$Cl]-based alkynyl complexes offer the potential for strong exchange coupling and well-isolated high-spin ground states.

EXPERIMENTAL SECTION

Preparation of Compounds. Manipulations were performed inside a dinitrogen-filled glovebox (MBRAUN Labmaster 130). Pentane was distilled over sodium metal and subjected to three freeze−pump−thaw cycles prior to use. Other solvents were sparged with dinitrogen, passed over alumina, and degassed prior to use. The preparations of [(dmpe)$_4$$Fe_2$$Cl_2$(μ-*p*-DEB)] (*p*-$H_2$DEB = 1,4-diethynylbenzene),[30] [(dmpe)$_2$FeCl(C_2Ph)],[30] [(dmpe)$_2$FeCl(C_2SiMe_3)](PF$_6$),[33] [(dmpe)$_4$$Fe_2$$Cl_2$(μ-*m*-DEB)],[33] [(dmpe)$_2$$FeCl_2$],[34] [$Cp_2$Fe]$BAr^F_4$ (Cp = η^5-C_5H_5; BAr^F_4 = tetrakis[3,5-bis(trifluoromethyl)phenyl]borate),[35] [Cp_2Fe]PF_6,[36] [Cp*$_2$Fe]PF_6,[36] and H_3TEB[37] have been described elsewhere. All other reagents were purchased commercially and used without further purification.

***trans*-[(dmpe)$_2$FeCl(C_2Ph)](OTf) (1).** A solution of AgOTf (33.4 mg, 0.130 mmol) in 5 mL of acetonitrile was added to a solution of [(dmpe)$_2$FeCl(C_2Ph)] (61.1 mg, 0.124 mmol) in 5 mL of dichloromethane. The solution color immediately turned dark-blue-green. The solution was stirred for 1 h and then filtered, and the filtrate was dried in vacuo. The resulting solid was recrystallized by slow diffusion of diethyl ether vapor into a concentrated solution of the crude product in dichloromethane. After 1 day, large dark-blue-green crystals were isolated by filtration, washed with diethyl ether (3 × 5 mL), and dried under vacuum for 1 h at 293 K to afford 65 mg of product (0.101 mmol, 82%). IR (mineral oil mull) $\nu_{C\equiv C}$: 2031 cm^{-1}. ^{1}H NMR (CD_2Cl_2): δ 27.85 (br, 2H, *m*-Ar−*H*), −20.35 (br, 16H, −PCH_3, −PCH_2), −23.74 (br, 12H, −PCH_3), −24.38 (br, 4H, −PCH_2), −27.32 (br, 2H, *o*-Ar−*H*), −28.06 (br, 1H, *p*-Ar−*H*). ESI-MS(+) (CH_2Cl_2): *m*/*z* 492 ([1 − OTf]$^+$). UV−vis (CH_2Cl_2) λ_{max}/nm (ε_M/M^{-1} cm^{-1}): 361 (sh, 4930), 411 (1240), 544 (sh, 800), 606 (3290), 732 (9490). Anal. Calcd for $C_{21}H_{37}ClF_3FeO_3P_4S$: C, 39.30; H, 5.81. Found: C, 39.30; H, 5.68.

[(dmpe)$_4$$Fe_2$$Cl_2$(μ-*p*-DEB)](BAr$^F_4$)$_2$ (2). A solution of [Cp_2Fe]BAr^F_4 (107 mg, 0.102 mmol) in 5 mL of dichloromethane was added to a solution of [Cl_2(dmpe)$_4$$Fe_2$(μ-*p*-DEB)] (46 mg, 0.051 mmol) in 5 mL of dichloromethane. The solution color immediately turned dark-green. After the solution was stirred for 10 min, the solvent was removed in vacuo. Pentane (5 mL) was added to precipitate a green solid. The solid was isolated by filtration, washed with pentane (3 × 5 mL) to remove residual [Cp_2Fe], and recrystallized by slow diffusion of pentane vapor into a concentrated solution of the crude product in dichloromethane. After 1 day, dark-green crystals were isolated by filtration, washed with pentane (3 × 3 mL), and dried under vacuum for 1 h at 293 K to afford 109 mg of product (0.041 mmol, 81%). Crystals suitable for X-ray analysis were obtained by allowing a solution of **2** in a 3:1 (v/v) pentane/dichloromethane mixture to stand in a −40 °C freezer for 3 days. IR (mineral oil mull) $\nu_{C\equiv C}$: 2017 cm^{-1}. ^{1}H NMR (CD_2Cl_2): δ 7.49 (br, 16H, BAr−*H*), 7.44 (br, 8H, BAr−*H*), −1.22 (br, 4H, Ar−*H*), −14.99 (br, 24H, −PCH_3), −15.22 (br, 8H, −PCH_2), −18.11 (br, 32H, −PCH_2, −PCH_3). UV−vis (CH_2Cl_2) λ_{max}/nm (ε_M/M^{-1} cm^{-1}): 403 (10 278), 475 (8442), 606 (4624), 747 (23 210), 837 (15 184). Anal. Calcd for $C_{98}H_{92}B_2Cl_2F_{48}P_8Fe_2$: C, 44.69; H, 3.52. Found: C, 44.47; H, 3.55.

[(dmpe)$_6$$Fe_3$$Cl_3$(μ$_3$-TEB)] (3). Freshly distilled triethylamine (0.2 mL, 1.43 mmol) was added to a solution of [(dmpe)$_2$$FeCl_2$] (117 mg, 0.274 mmol) and freshly sublimed H_3TEB (13.7 mg, 0.0913 mmol) in methanol (12 mL). The solution color immediately turned orange. After an additional 1 h of stirring, an orange solid precipitated. This solid was isolated by filtration, washed with methanol (3 × 3 mL) and pentane (3 × 3 mL), and then dried in vacuo for 1 h at 293 K to afford 52 mg of product (0.039 mmol, 43% based on H_3TEB). IR (mineral oil mull) $\nu_{C\equiv C}$: 2035 cm^{-1}. ^{1}H NMR (C_6D_6): δ 6.50 (s, 3H,

Table 1. Crystallographic Data[a] for the Compounds [(dmpe)$_2$FeCl(C$_2$Ph)](OTf) (1), [(dmpe)$_4$Fe$_2$Cl$_2$(μ-*p*-DEB)](BAr$^F_4$)$_2$ (2), and [(dmpe)$_6$Fe$_3$Cl$_3$(μ_3-TEB)](CF$_3$SO$_3$)$_3$ (4)[b]

	1	2	4
formula	$C_{21}H_{37}ClF_3FeP_8O_3F_3S$	$C_{98}H_{92}B_2Cl_2F_{48}Fe_2P_8$	$C_{50}H_{99}Cl_3F_6Fe_3O_6P_{12}S_2$
fw (g/mol)	641.75	2633.70	1619.97
color, habit	blue prism	green block	blue prism
T (K)	100(2)	100(2)	120(2)
space group	$P2_12_12_1$	$P\bar{1}$	*Pbcm*
Z	4	1	4
a (Å)	12.8296(3)	13.4127(7)	15.5873(6)
b (Å)	14.3749(4)	14.1127(7)	28.0448(12)
c (Å)	15.8508(4)	17.5241(10)	21.4267(10)
α (deg)	90	66.8130(10)	90
β (deg)	90	67.9560(10)	90
γ (deg)	90	81.356(2)	90
V (Å^3)	2923.3(1)	2826.3(3)	9366.5(7)
d_{calcd} (g/cm^3)	1.458	1.547	1.149
GOF	1.008	1.049	1.054
R_1[c] (wR_2)[d] (%) [$I > 2\sigma(I)$]	2.40 (5.40)	4.08 (10.45)	5.43 (17.83)

[a] Obtained with graphite-monochromatized Mo Kα radiation (λ = 0.71073 Å). [b] Data for [(dmpe)$_4$Fe$_2$Cl$_2$(μ-*m*-DEB)](BAr$^F_4$)$_2$ (**5**) are included in Table S1 in the SI. [c] $R_1 = \Sigma||F_o| - |F_c||/\Sigma|F_o|$. [d] $wR_2 = \{\Sigma[w(F_o^2 - F_c^2)^2/\Sigma[w(F_o^2)^2]\}^{1/2}$.

Ar−*H*), 1.60 (br, 24H, −PCH_2), 1.39 (br, 72H, −PCH_3). ^{31}P NMR (C$_6$D$_6$): δ 66.33 (s, 12P, Fe−*P*). ^{13}C NMR (C$_6$D$_6$): δ 130.26 (s, 3C, C_{Ar}H), 127.21 (s, 3C, C_{Ar}C≡C), 120.84 (s, 3C, C≡*C*−Fe), 84.82 (d, 3C, *C*≡C−Fe), 30.64 (p, 12C, CH_2), 16.02 (s, 12C, CH_3), 13.76 (s, 12C, CH_3). ESI-MS(+) (CH$_2$Cl$_2$): m/z 1320.00 ([**3**]$^+$). UV−vis (CH$_2$Cl$_2$) λ_{max}/nm (ε_M/M^{-1} cm^{-1}): 248 (122 500), 363 (77 500), 466 nm (1800). Anal. Calcd for $C_{48}H_{99}Cl_3P_{12}Fe_3$: C, 43.61; H, 7.55. Found: C, 43.34; H, 7.29.

[(dmpe)$_6$Fe$_3$Cl$_3$(μ_3-TEB)](OTf)$_3$ (4). To an orange slurry of **3** (30 mg, 0.023 mmol) in acetonitrile (10 mL) was added a solution of AgOTf (17.5 mg, 0.068 mmol) in acetonitrile (3 mL). The solution immediately turned blue-green. The mixture was stirred for 20 min and then filtered to remove silver metal, and the solvent was removed from the filtrate in vacuo. The solid was stirred with diethyl ether (10 mL) for 30 min at 293 K. The blue-green solid was isolated by filtration and recrystallized by slow diffusion of diethyl ether vapor into a concentrated solution of the crude product in dichloromethane. After 1 day, blue-green crystals were isolated by filtration, washed with diethyl ether (3 × 3 mL), and dried in vacuo for 1 h at 293 K to afford 34 mg of product (0.019 mmol, 83%). Although X-ray analysis suggested that as many as six molecules of dichloromethane are included in crystals of **4** (see below), samples for elemental analysis were sealed under vacuum, allowing the solvent to escape. IR (mineral oil mull) $\nu_{C\equiv C}$: 2035 cm^{-1}. ^{1}H NMR (CD$_2$Cl$_2$): δ 63.27 (br, 3H, Ar−*H*), −16.69 (br, 36H, −PCH_3), −18.07 (br, 12H, −PCH_2), −21.46 (br, 48H, −PCH_3, −PCH_2). ESI-MS(+) (MeCN): m/z 1617.80 ([**4** − OTf]$^+$), 735.57 ([**4** − 2OTf]$^{2+}$). UV−vis (CH$_2$Cl$_2$) λ_{max}/nm (ε_M/M^{-1} cm^{-1}): 301 (53 600), 401 (sh, 4290), 544 (sh, 1720), 609 (8100), 732 nm (12 940). Anal. Calcd for $C_{51}H_{99}Cl_3P_{12}F_9S_3O_9Fe_3$: C, 34.62; H, 5.64. Found: C, 34.58; H, 5.35.

[(dmpe)$_4$Fe$_2$Cl$_2$(μ-*m*-DEB)](BAr$^F_4$)$_2$ (5). A solution of [Cp$_2$Fe]-BAr$^F_4$ (52.3 mg, 0.050 mmol) in 5 mL of dichloromethane was added to a solution of [Cl$_2$(dmpe)$_4$Fe$_2$(μ-*m*-DEB)] (22.6 mg, 0.025 mmol) in 5 mL of dichloromethane. The solution color immediately turned dark-teal. After the solution was stirred for 10 min, the solvent was removed in vacuo. Pentane (5 mL) was added to precipitate a green solid. The solid was isolated by filtration, washed with pentane (3 × 5 mL) to remove residual [Cp$_2$Fe], and recrystallized by slow diffusion of pentane vapor into a concentrated solution of the crude product in dichloromethane. After 2 days, dark-blue crystals were isolated by filtration, washed with pentane (3 × 3 mL), and dried under vacuum for 1 h at 293 K to afford 53 mg of product (0.020 mmol, 80%). IR (ATR) $\nu_{C\equiv C}$: 2021 cm^{-1}. ^{1}H NMR (CD$_2$Cl$_2$): δ 46.85 (br s, 1H, Ar−*H*), 7.46 (s, 16H, BAr−*H*), 7.41 (s, 8H, BAr−*H*), −19.29 to −20.56 (br m, 32H, −PCH_3, −PCH_2), −21.93 to −22.54 (br m, 8H, −PCH_3, −PCH_2), −24.15 to −24.42 (br m, 24H, −PCH_3, −PCH_2), −55.79 (br s, 1H, Ar−*H*), −57.35 (br s, 2H, Ar−*H*). Anal. Calcd for $C_{98}H_{92}B_2Cl_2F_{48}P_8Fe_2$: C, 44.69; H, 3.52. Found: C, 44.93; H, 3.40.

X-ray Structure Determinations. Compounds **1**, **2**, **4**, and **5** were characterized by single-crystal X-ray analysis [Table 1 and Table S1 in the Supporting Information (SI)]. Crystals were coated in Paratone oil prior to removal from the glovebox, supported on Cryoloops, and mounted on a Bruker Kappa Apex 2 CCD diffractometer under a stream of cold dinitrogen. All data collections were performed with Mo Kα radiation and a graphite monochromator. Initial lattice parameters were determined from a minimum of 112 reflections harvested from 36 frames; these parameters were later refined against all data. Data sets were collected targeting complete coverage and fourfold redundancy. Data were integrated and corrected for absorption effects with the Apex 2 software package.[38] Structures were solved by direct methods and refined with the SHELXTL software package.[39] Displacement parameters for all non-hydrogen atoms were refined anisotropically with the exception of disordered carbon, phosphorus, and fluorine atoms. Hydrogen atoms were added at the ideal positions and refined using a riding model in which the isotropic displacement parameters were set at 1.2 times those of the attached carbon atom (1.5 times for methyl carbons). Two of the trifluoromethyl groups in the structure of **2** were disordered. The CF_3 disorder was modeled using a two-component treatment with an independent free variable for each group; the occupancies for each group refined to 85:15 and 79:21 ratios, respectively. After several attempts to model extreme anion/solvent disorder in the structures of **4** failed, the SQUEEZE routine in PLATON was applied.[40] For **4**, four 636 Å^3 voids were found; each contained 249 electrons. This electron count roughly corresponds to six dichloromethane molecules. The results for **4** presented in Table 1 reflect solvent-free data. Both of the triflate anions in the asymmetric unit of **4** reside on a mirror plane. Refinement of the

positional disorder in one of the triflates was modeled with a two-component model using a free variable. The occupancies of these two positions refined to a 70:30 ratio; with the exception of the sulfur atom, the minor component was refined isotropically. For the structure of **5**, the quality of the data was sufficiently low that only crude connectivity could be established (Figure S1 in the SI). Crystal data for **5** are presented in the SI.

Magnetic Susceptibility Measurements. Magnetic susceptibility data were collected with a Quantum Design MPMS-XL SQUID magnetometer. In the glovebox, finely ground samples were loaded into gelatin capsules and inserted into straws. The straws were sealed in plastic bags prior to removal from the glovebox and quickly loaded into the instrument to minimize exposure to air. Data were corrected for the magnetization of the sample holder by subtracting the susceptibility of an empty container and for diamagnetic contributions of the sample by using Pascal's constants.[41] Theoretical fits to the susceptibility data for **2** and **5** were obtained using a relative error minimization routine (julX 1.4.1)[42] with a Hamiltonian of the form $\hat{H} = -2J\hat{\mathbf{S}}_1 \cdot \hat{\mathbf{S}}_2$. The best fits to the data for trinuclear **4** were obtained with MAGFIT 3.1[43] using a three-center isosceles spin Hamiltonian of the form $\hat{H} = -2J(\hat{\mathbf{S}}_1 \cdot \hat{\mathbf{S}}_3) - 2J(\hat{\mathbf{S}}_2 \cdot \hat{\mathbf{S}}_3) - 2J'(\hat{\mathbf{S}}_1 \cdot \hat{\mathbf{S}}_2)$.

Other Physical Measurements. Electronic absorption spectra were obtained in air-free cuvettes with a Hewlett-Packard 8453 spectrophotometer. IR spectra were measured with a Nicolet 380 FT-IR spectrophotometer using either mineral oil mulls sandwiched between NaCl plates or a Smart Performer ZnSe attenuated total reflectance (ATR) accessory. ^{1}H NMR spectra were recorded on a Varian INOVA instrument operating at 300 MHz. Electron paramagnetic resonance (EPR) spectra were obtained using a continuous-wave X-band Bruker EMX 200U instrument outfitted with a liquid nitrogen cryostat. Compounds were dissolved in a 1:1 mixture of dichloromethane and 1,2-dichloroethane to form a glass at low temperature. Cyclic voltammetry experiments were done in 0.1 M solutions of $(Bu_4N)PF_6$ in dichloromethane. Cyclic voltammograms (CVs) were recorded with a CH Instruments potentiostat (model 1230A or 660C) using a 0.25 mm Pt disk working electrode, Ag/Ag^+ reference electrode, and Pt mesh auxiliary electrode. All CVs shown were measured at a scan rate of 0.1 V/s. Reported potentials are referenced to the $[Cp_2Fe]^+/[Cp_2Fe]$ (Fc^+/Fc) redox couple and were determined by adding ferrocene as an internal standard at the conclusion of each electrochemical experiment. Elemental analyses were performed by Robertson Microlit Laboratories (Madison, NJ).

Electronic Structure Calculations. In general, unrestricted B3LYP hybrid DFT studies[44] and time-dependent DFT (TD-DFT)/natural transition orbital (NTO) analyses were carried out using the Gaussian 09 suite of electronic structure codes.[45] Given the presence of low-lying excited states, difficult-to-converge wave functions were converged using a quadratically convergent procedure.[46] The possible presence of lower-energy wave function solutions was investigated using a stability check protocol.[47] LANL2[48] basis sets and effective core potentials were used for Fe and P atoms; the 6-31G* or polarized Dunning valence double-ζ basis sets were used for the remaining atoms, as noted.[49−52] For $[(dmpe)_6Cl_3Fe_3(TEB)]^{3+}$ (the cation of **4**), geometries for four idealized (P···P centroid−Fe)−(phenyl plane) orientational isomers (having different values of the torsion angle φ defined in Figure 2c) were optimized for the quartet ground state. Except as noted, the optimization studies used Fe−P distances constrained to 2.28 Å. For $[(dmpe)_4Cl_2Fe_2(p\text{-DEB})]^{2+}$ (the cation of **2**) and $[(dmpe)_4Cl_2Fe_2(m\text{-DEB})]^{2+}$ (the cation of **5**), geometries were optimized for the lowest-energy (P···P centroid−Fe)−(phenyl plane) orientational isomers. For $[(dppe)_3(Cp^*)_3Fe_3(TEB)]^{3+}$, two structures were considered: for the first, the coordinates from the Fe(II) crystal structure[53] were used with C(sp^3)−H bonds set to 1.09 Å and C(sp^2)−H bonds set to 1.07 Å, and C−C bond distances for the alkynylaromatic bridging framework were symmetrized; for the second, the [(dppe)(Cp*)Fe] fragments were rotated about the (P···P centroid)−Fe−(phenyl plane) dihedral angle φ (see Figure 2c for definition) to align the magnetic orbitals with the aryl π system. For the series of $[(dXpe)_6Cl_3Fe_3(TEB)]^{3+}$ complexes, the geometry was optimized for X = H [i.e., for 1,2-diphosphinoethane (dpe)]; X−C bond distances were fixed at idealized values.

The current three-center, three-electron doublet system is difficult to compute with standard literature techniques. The broken-symmetry projection approaches of Noodleman[54] and Soda[55] are problematic here: the present systems contain three low-spin broken-symmetry states ($\alpha\alpha\beta$, $\alpha\beta\alpha$, and $\beta\alpha\alpha$, corresponding to placing the β spin on each of the three Fe centers) but only two actual doublets. Sum rules[56] and spin-flip[57−59] approaches are appropriate when the individual determinants are degenerate (not generally true) but do not treat coupling between the two doublet states. To estimate the magnetic interactions, the high-spin quartet and three $M_S = {}^1/_2$ spin-flip "doublet" microstates were computed. Spin natural orbitals derived from the ground-state quartet were used to generate starting guesses for the three possible single-spin-flip $M_S = {}^1/_2$ states for each of the trinuclear complexes. Magnetic J values were estimated using eqs 2−4, and the energy differences are defined in eqs 5−7. Further details are provided in the SI.

$$J_{13} = \frac{1}{2}\left(\Delta E_{\alpha\alpha\beta} - \Delta E_{\alpha\beta\alpha} + \Delta E_{\beta\alpha\alpha}\right) \tag{2}$$

$$J_{23} = \frac{1}{2}\left(\Delta E_{\alpha\alpha\beta} - \Delta E_{\beta\alpha\alpha} + \Delta E_{\alpha\beta\alpha}\right) \tag{3}$$

$$J_{12} = \frac{1}{2}\left(\Delta E_{\alpha\beta\alpha} - \Delta E_{\alpha\alpha\beta} + \Delta E_{\beta\alpha\alpha}\right) \tag{4}$$

$$\Delta E_{\alpha\alpha\beta} = E_{\alpha\alpha\beta} - E_{\alpha\alpha\alpha} \tag{5}$$

$$\Delta E_{\alpha\beta\alpha} = E_{\alpha\beta\alpha} - E_{\alpha\alpha\alpha} \tag{6}$$

$$\Delta E_{\beta\alpha\alpha} = E_{\beta\alpha\alpha} - E_{\alpha\alpha\alpha} \tag{7}$$

The quartet and doublet energies were obtained from eqs 8 and 9, respectively:

$$E_Q = -\frac{1}{2}\left(J_{12} + J_{13} + J_{23}\right) \tag{8}$$

$$E_{D_1/D_2} = \frac{1}{2}\left(J_{12} + J_{13} + J_{23} \pm 2\sqrt{J_{12}^2 + J_{23}^2 + J_{13}^2 - J_{12}J_{13} - J_{12}J_{23} - J_{13}J_{23}}\right) \tag{9}$$

It should be noted that when $J_{12} = J_{13} = J$ and $J_{23} = \gamma J$, the doublet energies reduce to the literature expressions[60−62] $E_{D_1} = 2J - \gamma J$ and $E_{D_2} = {}^3/_2\gamma J$. When $J_{12} = J_{13} = J_{23} = J$, the doublet energies simplify further to $E_{D_1/D_2} = {}^3/_2 J$.

The relative stabilities and characters of the five d orbitals of each magnetic iron center were assessed using a TD-DFT/NTO analysis of the mononuclear fragments $[(dmpe)_2FeCl(C_2H)]^+$, $[(dmpe)_2ClFe(C_2Ph)]^+$ (the cation of **1**), and $[(dppe)(Cp^*)Fe(C_2Ph)]^+$. Fragment geometries were extracted from the trinuclear complexes, with the exception that the Fe−C distance was varied from 1.800 to 2.300 Å for $[(dppe)(Cp^*)Fe(C_2Ph)]^+$ and from 1.907 to 2.397 Å for $[(dmpe)_2ClFe(C_2Ph)]^+$ for two dmpe rotamers, one parallel and the other perpendicular to the phenylacetylide aromatic ring.

RESULTS AND DISCUSSION

Syntheses and Characterizations. The preparations of the di- and triethynylbenzene-bridged complexes are outlined in

Scheme 1. Syntheses of Ethynylbenzene Complexes 1−5

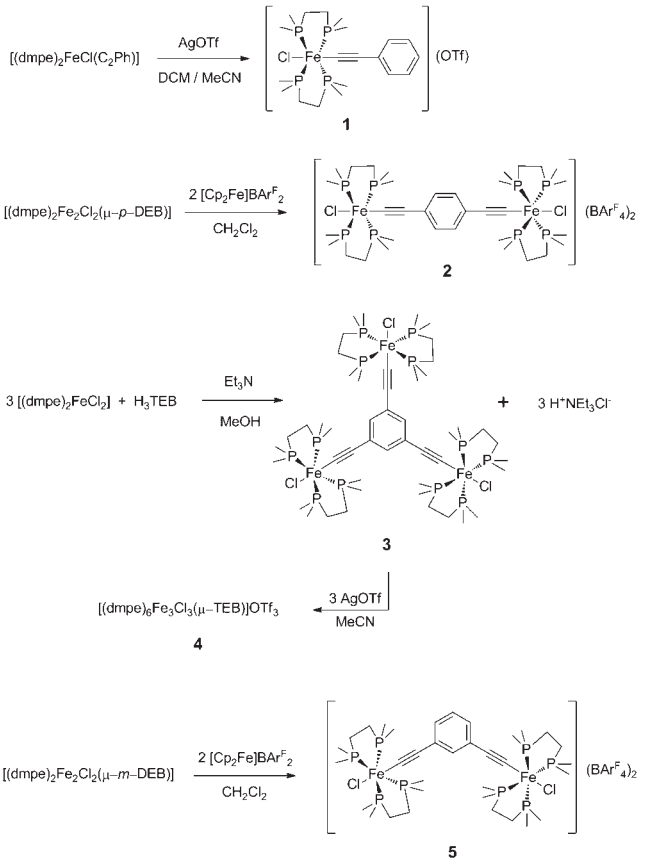

Scheme 1. The neutral (diferrous) form of complex **2**, $[(dmpe)_4Fe^{II}{}_2Cl_2(p\text{-DEB})]$, was previously described by Field and co-workers;[30] the synthesis of the trinuclear complex **3** was adapted from that report. The hexafluorophosphate analogue of **5**, $[(dmpe)_4Fe^{II}{}_2Cl_2(p\text{-DEB})](PF_6)_2$, has been synthesized by Berben,[33] and a similar synthetic procedure was adopted here. Related compounds with (Cp*)(dppe)Fe units coordinated to bridging ethynylbenzene ligands have also been reported by Lapinte.[19,23,53,63] For the preparation of the ferrous compounds, Field and co-workers' efforts indicated that $[(dmpe)_2FeCl_2]$ undergoes solvolysis in methanol to generate $[(dmpe)_2Fe(MeOH)Cl]^+$, which interacts with the ethynylbenzene ligand, presumably forming a vinylidene complex. The vinylic proton is then captured by triethylamine to form the iron acetylide complex product, which precipitates cleanly from the reaction mixture. The purity of **3** was verified by combustion analysis, mass spectrometry, and ^1H, ^{31}P, and ^{13}C NMR spectroscopy (Figures S2−S4, respectively, in the SI). The ^1H NMR spectrum contains a sharp resonance corresponding to the aromatic protons in addition to broad resonances from the ethylene and methyl protons of the dmpe ligands. A single sharp resonance in the ^{31}P spectrum confirms the trans coordination geometry about each Fe(II) ion.

Cyclic voltammetry studies afford the potentials required for oxidation to Fe^{III} species and serve as a probe of the electronic coupling between iron ions. CVs for the ferrous complexes $[(dmpe)FeCl(C_2Ph)]$,[30] $[(dmpe)_4Fe_2Cl_2(\mu\text{-}p\text{-DEB})]$,[30] and $[(dmpe)_4Fe_2Cl_2(\mu\text{-}m\text{-DEB})]$[33] have been reported by Field and Berben; the CVs for the corresponding ferric complexes **1**, **2**, and **5** are identical to those except for the value of the rest potential, consistent with oxidation of Fe^{II} to Fe^{III}.

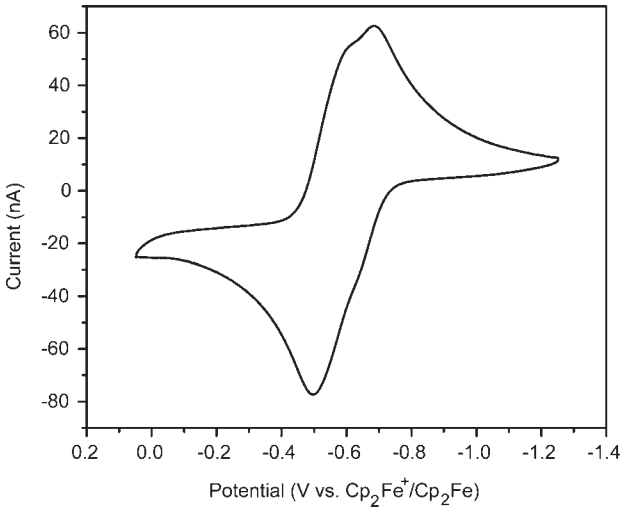

Figure 1. Cyclic voltammogram of **3** in dichloromethane.

The previously reported electrochemical behavior of $[(dmpe)_4Fe^{II}{}_2Cl_2(\mu\text{-}p\text{-DEB})]$ shows two reversible one-electron redox waves centered at −0.69 and −0.49 V vs Fc^+/Fc.[30] These waves correspond to the formation of the mixed-valent $[Fe^{III}Fe^{II}]$ and diferric $[Fe^{III}Fe^{III}]$ complex cations in solution. Interestingly, the comproportionation constant is much larger for $[(dppe)_2(Cp^*)_2Fe_2(p\text{-DEB})]^{n+}$ ($K_{com} = 2.6 \times 10^4$)[63] than for $[(dmpe)_4Cl_2Fe_2(p\text{-DEB})]^{n+}$ ($K_{com} = 2.4 \times 10^3$), indicating stronger Fe−Fe electronic communication in the Cp*-ligated species. On the basis of the CV data, the $BAr^F{}_4$ salt **2** can be prepared by oxidizing the neutral $[Fe^{II}{}_2]$ complex with 2 equiv of $[Cp_2Fe]PF_6$.

For the trinuclear complexes, Lapinte and co-workers previously reported the isolation of mono- and diferric derivatives of $[(dppe)_3Fe_3(Cp^*)_3TEB)]^{n+}$ complexes on the basis of the presence of three well-separated redox waves ($\Delta E_{1/2} = 0.130$ V) for the neutral complex in dichloromethane solution.[53,30] The *m*-phenylene bridges in **3** and **5** would be expected to engender weaker coupling than the *p*-phenylene and Cp* variants[53,63] because of the lack of cumulenic/quinoidal character in the overall bonding structure for complexes with an *m*-DEB bridge.[25,64] Indeed, the CV for **3** shows one broad redox wave centered at −0.59 V with a peak-to-peak separation of 186 mV (Figure 1). The appearance of shoulders at ca. −0.61 and −0.64 V indicates that multiple redox processes occur on the electrochemical time scale, but the lack of resolution is consistent with weaker communication between metal centers, similar to the behavior observed for the dinuclear complexes. On the basis of the electrochemical data, the triferric complex **4** can be synthesized by combining **3** with 3 equiv of AgOTf in acetonitrile. The purity of **4** was confirmed by microanalysis and ^1H NMR spectroscopy. The ^1H NMR spectrum contains broad, paramagnetically shifted peaks from aromatic, methyl, and ethylene protons, and resonances from precursor **3** are not present in the ^1H NMR spectrum of **4** (Figure S5a in the SI). The mononuclear ferric complex **1** was prepared in a similar fashion.

All of the compounds were characterized by FT-IR spectroscopy. As a result of π back-bonding from iron, the ethynylbenzene-bridged complexes exhibit a single $\nu_{C\equiv C}$ resonance at lower

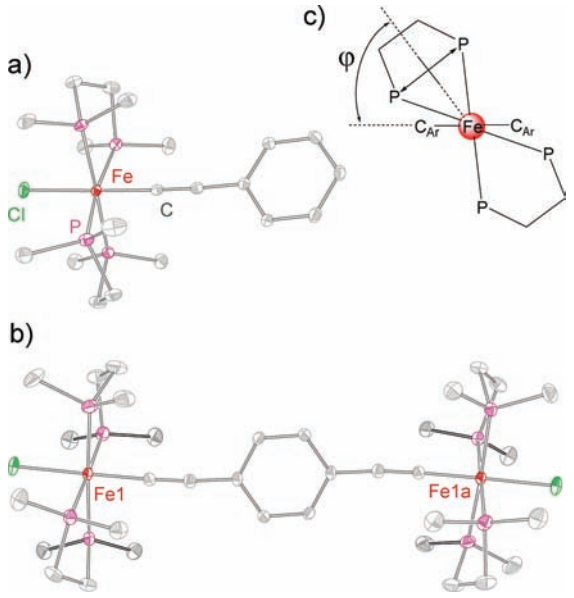

Figure 2. X-ray structures of the complex cations in (a) **1** and (b) **2**, with red, purple, green, and gray ellipsoids/spheres corresponding to Fe, P, Cl, and C atoms, respectively. Thermal ellipsoids are rendered at 40% probability. H atoms in all structural plots have been omitted for clarity. A rendering for **5** is presented in Figure S1 in the SI. (c) Definition of the torsion angle φ as viewed down the Cl−Fe−C axis; Cl has been omitted for clarity.

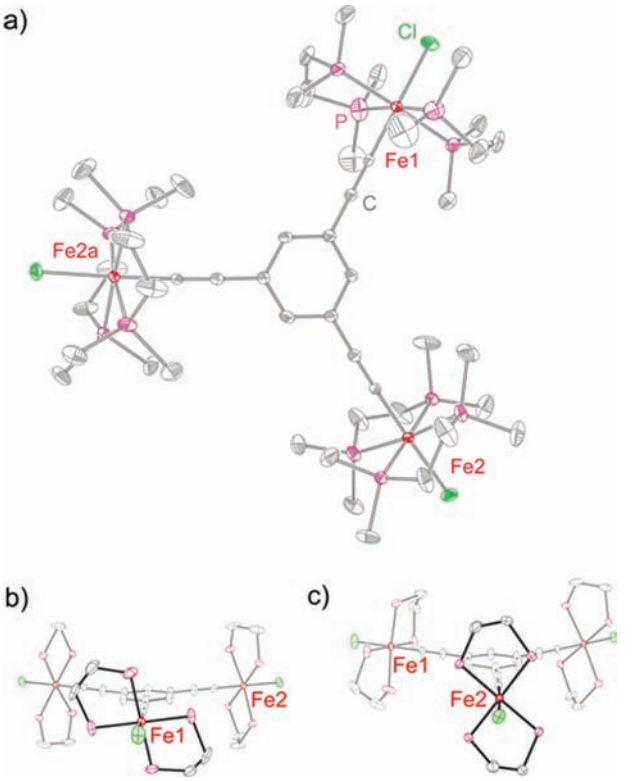

Figure 3. (a) X-ray structure of the complex cation in **4**, with H atoms removed for clarity. (b, c) Views of the cation along the (b) Cl1−Fe1−C_2 and (c) Cl2−Fe2−C_2 axes, with H atoms and methyl groups omitted for clarity. See Figure 2 for color coding. All thermal ellipsoids are rendered at 40% probability.

energies relative to the free acetylene compounds. The acetylide stretching frequency in **2** decreases to 2017 cm^{-1} versus 2042 cm^{-1} in the neutral complex. Coincidentally, the acetylide stretches for redox-related **3** and **4** both occur at 2035 cm^{-1}.

As expected, orange solutions of ferrous **3** quickly turn blue-green in air, indicating oxidation of the Fe^{II} centers to Fe^{III}. In the solid state, ferric **1**, **2**, **4**, and **5** maintain their structural connectivity in air for period of at least 1 day, as determined by IR spectroscopy. A gradual change in color upon exposure to air for dichloromethane solutions of ferric **1**, **2**, **4**, and **5** from blue-green to green was observed over several days; the identities of the decomposition products were not determined.

X-ray Structures. The crystal structures of all of the complexes presented herein reveal a pseudo-octahedral coordination geometry around each iron center (Figures 2 and 3). The equatorial positions are occupied by four phosphorus atoms from the bidentate dmpe ligands, while the chloride and bridging-acetylide-containing ligands are located at the axial positions. The acetylide ligands in the cations of all of the structures impart a rigid connectivity, leading to essentially linear C−C−Fe angles; the greatest deviation from linearity is 2.8° in the structure of **2**. The average Fe−C bond lengths are 1.8750(12), 1.871(2), and 1.876(6) Å for complexes **1**, **2**, and **4**, respectively. Other relevant bond distances and angles are comparable to those of related complexes in the literature.[24,29,63,65]

For **4**, two of the Fe atoms (Fe2 and Fe2a) are related by a crystallographic twofold rotation axis, and the ethylene carbon atoms of their bidentate dmpe ligands are essentially parallel to the plane of the aromatic bridging ligand. The torsion angle φ, defined by the P···P centroid, the Fe ion, and the two adjacent carbon atoms on the central aromatic ring, is 82.2° (see Figure 2c for pictorial definition of φ). In contrast to the environment around Fe2 and Fe2a, the dmpe ligands coordinated to Fe1 are roughly perpendicular to the central phenyl ring (φ = 36.9°). The Fe atoms reside at the vertices of an isosceles triangle; the Fe1···Fe2 and Fe1···Fe2a distances are 10.184(1) Å, while the Fe2···Fe2a distance is 10.389(1) Å. Examination of the packing plot (Figure S6 in the SI) reveals that the cationic complexes are arranged in two-dimensional layers parallel to the crystallographic *ab* plane. These arrays are separated from one another by triflate anions, and the interlayer distance as measured from the aromatic ring is ∼10.713(2) Å. When viewed down the *c* axis, the cations form infinite stacks that are perfectly eclipsed. The shortest cation−anion distance is 3.3(3) Å and it occurs between one of the Fe1 dmpe ethylene carbons (C14) and an oxygen atom from one of the triflates (O1). The large estimated standard deviation for this interatomic distance is likely the result of libration effects in the triflate molecule. While this is not an obvious hydrogen-bonding interaction, the packing effect nevertheless appears to influence the orientation of the dmpe ligands on Fe1, causing them to be twisted out of registry with respect to the dmpe ligands coordinated to Fe2 and Fe2a.

The structure solution for compound **5** established the atomic connectivity and provided an estimate of relevant structural metrics. However, the relatively poor resolution for crystals of **5** precluded a rigorous analysis of bond lengths from the X-ray data, and the presence of dmpe ligand disorder could not be ruled out. Similar crystallographic challenges were encountered by Berben in the disclosure of the structure of the hexfluorophosphate analogue of **5**.[15]

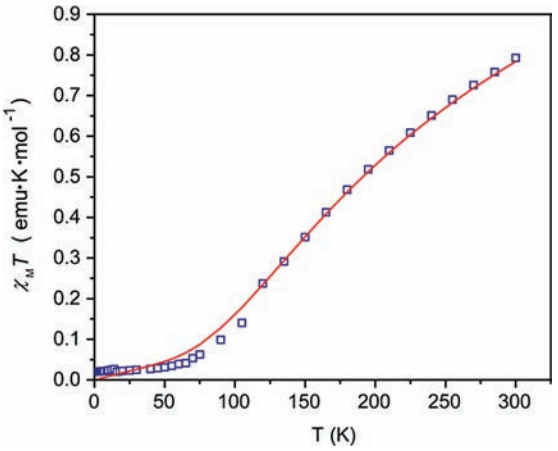

Figure 4. Temperature-dependent magnetic susceptibility data for **2** (blue □) and the best fit (solid red line).

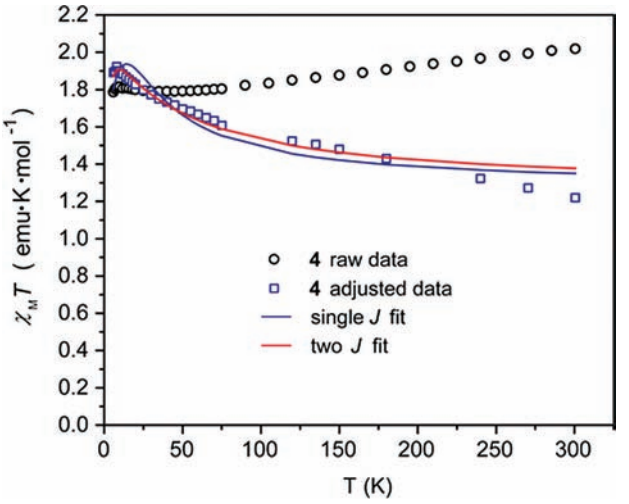

Figure 5. Raw and TIP-corrected magnetic susceptibility data for **4** obtained in a 1 kOe dc field, including best-fit lines from one- and two-J coupling models. See the text for details of the data adjustment and fitting procedures. Susceptibility values for $[(dmpe)_2FeCl(C_2SiMe_3)](PF_6)$ at 90, 105, 195, 210, and 225 K were not available for generating adjusted data points.[33]

Magnetic Properties. The magnetic susceptibilities (χ_M) for all of the Fe^{III}-containing compounds presented here (Figures 4−6 and Figure S13 in the SI) show significant temperature-independent paramagnetism (TIP), manifested as a linear increase in $\chi_M T$ with increasing temperature and higher-than-expected room-temperature susceptibilities for the compounds assuming $g = 2.00$. This issue has been noted previously for pseudo-octahedral Fe^{III} complexes, and its origin has been attributed to either unquenched orbital angular momentum or small amounts of paramagnetic iron impurities present in the sample.[18,22] Considering that we used crushed crystalline samples for magnetic measurements and obtained consistent results from multiple samples prepared at different times, we believe that we minimized the paramagnetic impurities, so the magnetic interpretations to be presented reflect intrinsic properties of the compounds.

The dichloromethane/dichloroethane frozen glass X-band EPR spectra of mononuclear **1**, dinuclear **2**, and trinuclear **4** show broad, axial signals at 100−110 K (Figures S8−S10 in the SI). The signals for **2** represent the triplet excited state rather than the diamagnetic singlet ground state: they are similar to resonances observed for trinuclear **4**, albeit much weaker. Detailed analyses of the spectra for the multinuclear complexes are complicated by exchange coupling and the relative orientations of the Fe^{III}-containing units and will be discussed in a future report. To find a reasonable "isotropic" g value for anchoring the magnetic susceptibility data fits for the meta-bridged species **4** and **5**, we analyzed the EPR spectrum of the mononuclear phenylacetylide complex salt **1** using the EasySpin software package.[66] The simulated spectrum that best matched the data gave the parameters $g_x = 1.9419$, $g_y = 1.9415$, and $g_z = 2.5681$ and a Lorentzian line width of 75.31 mT. The average of the g_x, g_y and g_z values is 2.150 (Figure S8 in the SI).

The susceptibility data for the para-bridged dinuclear complex **2** are presented in Figure 4. The $\chi_M T$ value of 0.79 emu K mol^{-1} at 300 K is just slightly higher than the value of 0.75 emu K mol^{-1} expected for two uncoupled $S = {}^1/_2$ centers with $g = 2.00$). As the temperature is decreased, $\chi_M T$ decreases steadily to 0.07 emu K mol^{-1} at 75 K and then drops more gradually to 0.02 emu K mol^{-1} at 4 K. The trend exhibited by **2** indicates that antiferromagnetic (AF) coupling is operative. In the phenomenological fitting protocol, we found that the g and TIP are correlated in such a way that smaller g values are countered by large TIP values and vice versa, all yielding comparable fits to the experimental data, with minor effects on the magnitude of J (see Table S2 in the SI for more details). When a small amount of paramagnetic impurity was included to account for the nonzero $\chi_M T$ product below 50 K ($S = {}^1/_2$, 2.1%), the best fit to the raw data afforded $J = -134$ cm^{-1} with $g = 2.34$ and TIP fixed at 600×10^{-6} emu. While this coupling constant is robust, it is significantly smaller than that reported for similar Cp*-ligated complexes.[24,25] The differences in ligands for the complexes discussed here likely influence the propensity of the Fe^{III} ion to form Fe═C-type interactions.[22] In addition, the relative orientations of the "magnetic" d orbitals with respect to the aromatic π system influence the observed J couplings; this will be explored in more detail below.

For trinuclear **4** (Figure 5), the classical curve shape for a ferromagnetically coupled system is obscured by the apparent involvement of unquenched orbital angular momentum. The susceptibility decreases from 2.00 emu K mol^{-1} at 300 K to a local minimum of 1.79 emu K mol^{-1} at 40 K, followed by an increase to 1.82 emu K mol^{-1} at 10 K. Below 10 K, the susceptibility drops off rapidly, which may be due to a combination of weak intermolecular AF interactions, Zeeman splitting, and/or zero-field splitting effects. The value of $\chi_M T$ at 10 K is slightly smaller than the spin-only value expected for a ferromagnetically coupled $S = {}^3/_2$ system with $g = 2$ (1.875 emu K mol^{-1}).

A similar picture emerges from the raw data for dinuclear **5** (Figure 6). At 300 K, $\chi_M T$ is 1.67 emu K mol^{-1}. Cooling the sample results in a monotonic susceptibility decrease to 1.15 emu K mol^{-1} at 40 K. Below 7 K, a more rapid decrease occurs, and $\chi_M T$ is 1.06 emu K mol^{-1} at 2 K.

To obtain a proper evaluation of the extent of magnetic communication between the metal centers in **4** and **5**, it was useful to remove unquenched orbital angular momentum contributions from the raw data to isolate the spin-only and exchange contributions. It should be noted that these contributions, which

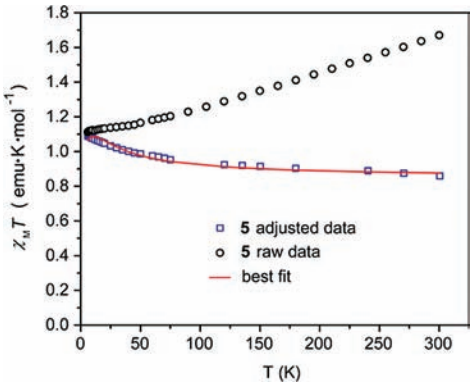

Figure 6. Raw and corrected magnetic susceptibility data for **5** collected in a 1 kOe dc measuring field. See the text for details of the data adjustment and fitting procedures. Susceptibility values for $[(dmpe)_2FeCl(C_2SiMe_3)](PF_6)$ at 90, 105, 195, 210, and 225 K were not available for generating adjusted data points.[33]

arise from the spin−orbit coupling brought about by near-degenerate electronic configurations for each of the Fe^{III} centers, were also likely present in **2**. However, the effects appeared to be quenched by the strong intramolecular AF interaction. The orbital contributions of the low-spin Fe^{III} ions in compounds **4** and **5** were eliminated from the data by the following protocol: *n* equivalents of the susceptibility for $[(dmpe)_2FeCl(C_2SiMe_3)](PF_6)$[33] were subtracted from the raw data, and then the ligand susceptibility and the expected spin-only value for *n* low-spin d^5 centers with $g = 2.15$ were added ($n = 3$ for **4** and 2 for **5**). Similar procedures have previously been applied to magnetic data for Fe^{III}-containing species in order to evaluate more accurately the magnetic coupling interactions in systems where masking effects were present.[33,67−70] Further details are provided in the SI.

The resulting plot for dinuclear **5** (Figure 6) shows temperature-dependent magnetic behavior in line with the expected ferromagnetic coupling of low-spin Fe^{III} ions. The value of $\chi_M T$ at 300 K is 0.77 emu K mol^{-1}, corresponding to two uncoupled electrons with a *g* value slightly larger than 2. The susceptibility gradually increases upon cooling, reaching a maximum value of 0.98 emu K mol^{-1} at 6 K. This behavior is entirely consistent with an $S = 1$ ground state at low temperature. Unlike the para-bridged compound **2**, where the raw data were used for fitting, *g* and *J* are inversely correlated for the corrected data fit for **5**. Thus, gaining insight is possible only when one of the values can be determined independently. Analysis of the EPR spectrum for mononuclear **1** (Figure S8 in the SI) afforded an independent determination of g_{iso}. Fitting the data with *g* fixed at 2.15 afforded $J = +11$ cm^{-1}. In the fit, a small mean-field correction (−0.48 K, −0.3 cm^{-1}) accounts for very weak AF interactions between dinuclear complexes. The data for **5** are comparable to those for $[(dmpe)_4Fe_2Cl_2(\mu\text{-}m\text{-DEB})](PF_6)_2$ obtained by Berben.[33] The magnetic susceptibility data for both compounds were treated identically, yet *J* for the hexafluorophosphate salt is +41 cm^{-1}, significantly higher than the value found for **5**. X-ray structural data for $[(dmpe)_4Fe_2Cl_2(\mu\text{-}m\text{-DEB})](PF_6)_2$ were not available for detailed analysis, but the ancillary ligand conformations appear to be similar to those in **5**.[33] Comparison to Cp*-containing *m*-DEB-bridged Fe^{III} systems is also telling: coupling constants in those molecules range from 65 cm^{-1} to apparently >150 cm^{-1}.[19,25,71] It should be noted that the subtraction−replacement protocol used to analyze the magnetic properties of **5** provides a *lower-bound estimation* of *J*.[67]

The adjusted data for **4** (Figure 5) also show the expected ferromagnetic coupling of Fe^{III} centers. The $\chi_M T$ value at 300 K is 1.07 emu K mol^{-1}, which is near the value expected for three uncoupled $S = {}^1/_2$ centers with *g* near 2.00 (1.13 emu K mol^{-1}). The susceptibility increases gradually upon cooling, reaching a maximum of 1.77 emu K mol^{-1} at 8 K, and then decreases slightly to 1.74 emu K mol^{-1} at 5 K. Considering that the Fe^{III} ions are located at the vertices of an isosceles triangle and that one of the $(dmpe)_2Fe^{III}$ groups is twisted out of registry with respect to the other two, we fit the data assuming two different exchange coupling constants. The best fits to the 2*J* model gave $J_{12} = J_{13} = 5$ cm^{-1} and $J_{23} = 37$ cm^{-1} with *g* constrained at 2.15; a small mean-field correction (−0.84 K, −0.58 cm^{-1}) accounts for very weak AF interactions between dinuclear complexes. Treating the data with a single exchange coupling constant between 6 and 300 K yielded a significantly different *J* value ($J = 12$ cm^{-1}; $g = 2.15$) and a much poorer fit, especially at low temperature. Comparison to structurally and magnetically characterized organic triradicals is meaningful: Iwamura applied an isosceles model to the susceptibility data for 2-methoxy-1,3,5-benzenetriyltris(*N-tert*-butylnitroxide) and obtained $J_{12} = J_{13} = 48$ cm^{-1} and $J_{23} = 3$ cm^{-1}.[62] Interestingly, the fit to the data for **4** indicates significantly stronger magnetic coupling than determined for the Cp*-containing TEB-bridged triiron complex, where the two *J* values were reported to be 9.6 and 4.4 cm^{-1}.[65] The geometric and electronic origins of this behavior are explored in the next section.

Magnetization data collected in direct current (dc) fields up to 5 T support the assignment of an $S = {}^3/_2$ ground state for **4** (Figure S7 in the SI), as the magnetization appears to saturate at $\sim 3\, N\mu_B$. The presence of axial magnetic anisotropy is evidenced by a slight non-overlap of the isofield lines and tracking of all of the magnetization data below the Brillouin function predicted for $S = {}^3/_2$, $g = 2.13$. For comparison, a slight non-superposition of isofield lines was observed by Holland and co-workers[72] in a low-coordinate Fe(II) complex: there it was reported that both $|D|$ and $|E|$ were very large ($E \approx D/3$). Preliminary alternating current (ac) susceptibility studies for **4** carried out at zero applied dc field showed no frequency dependence in the out-of-phase susceptibility component, indicating that at least at zero applied dc field, **4** does not behave as an SMM.

Magnetostructural Correlations in the TEB-Bridged Complexes. A comparison of the electrochemical data for **3** and $[(dppe)_3(Cp^*)_3Fe_3(TEB)]$ suggests that electronic communication between the Fe ions should be much weaker in the former complex. We might expect that to translate into weaker magnetic coupling for **4** versus $[(dppe)_3(Cp^*)_3Fe_3(TEB)]^{3+}$. For related acetylide and nitrile-containing dinuclear complexes, it has been argued that *J* scales with the amount of spin that is delocalized on the bridging ligand.[25,73] While this may explain the behavior of *p*-DEB-bridged species, where the cumulenic form can be transmitted across the bridge, it is not as helpful for the *m*-DEB- and TEB-bridged complexes, where such resonance structures are not supported. Notwithstanding, the coupling in trinuclear **4** is clearly much stronger than that found in the Cp-containing species. In the following, our aims are to explore the magnetostructural correlations in the *m*/*p*-DEB- and TEB-bridged Fe^{III} systems and come to a general understanding of spin delocalization in ethynylbenzene-bridged complexes.

Although the crystallographic twofold symmetry in the structure of **4** justifies use of a two-*J* fitting model, the more significant contribution to the ferromagnetic coupling in the trinuclear complex originates from orbital symmetry considerations. Lapinte and co-workers have interpreted the AF coupling in polyenediyl-bridged diradicals using criteria developed by Borden, where the degree of overlap between metal dπ and ligand π orbitals has a large influence on the sign and magnitude of magnetic exchange.[24,27,60,74] Berke has nicely illustrated the dependence of the singlet−triplet energy gap on the relative orientation of the spin centers in a Mn_2C_2 complex.[28] However, correlation of the exchange to the geometry has not been considered in detail for the ethynylbenzene-bridged systems.

As described in the SI, a number of computational studies have been carried out to probe the nature of bridge-mediated magnetic coupling, the first being a TD-DFT/NTO analysis of the mononuclear fragment $[(dmpe)_2FeCl(C_2H)]^+$ (Figure S14 in the SI). With a B3LYP LANL2/6-31 g* hybrid density functional, the ground state was found to possess a low-spin d^5 configuration with one member of the "t_{2g}" set singly occupied. This magnetic orbital is has π symmetry with respect to the four phosphorus centers and is directed between the chelate rings (interchelate). The lowest-energy excitation takes an electron from the doubly occupied perpendicular dπ orbital (intrachelate) and places it in the singly occupied dπ orbital; this excited state is computed to be 7 kcal/mol above the ground state. Since this energy roughly corresponds to a 2700 T applied field, the only magnetically accessible state places the unpaired electron in a dπ orbital directed between the chelate rings. To probe the impact of the bridging phenyl ring, the above-mentioned TD-DFT/NTO analysis was repeated for $[(dmpe)_2FeCl(C_2Ph)]^+$ as a function of the Fe−C distance and the orientation (φ = 0 and 90°). When φ = 0°, the interchelate dπ orbital is aligned with the phenyl π system, whereas when φ = 90°, the intrachelate dπ orbital is aligned with the phenyl π system. For φ = 0°, the interchelate dπ orbital was computed to remain singly occupied in the ground state as the Fe−C distance was varied from 1.907 to 2.397 Å (Figure S15a in the SI). For φ = 90°, the intrachelate dπ orbital was computed to be singly occupied in the ground state for short Fe−C distances (d_{Fe-C}) from 1.907 to roughly 2.020 Å (Figure S15b). For d_{Fe-C} > 2.020 Å, the ground state reverts to the configuration wherein the interchelate dπ orbital is magnetic (Figure S15c). When d_{Fe-C} = 1.907 Å, the intrachelate dπ orbital configuration is favored by nearly 7 kcal/mol, whereas when d_{Fe-C} = 2.397 Å, the singly occupied interchelate dπ orbital configuration is favored by nearly 8 kcal/mol (Figure S15d). Thus, for short Fe−C distances, the dπ interaction with the aromatic π system dominates, while at longer Fe−C distances this interaction is diminished and ancillary ligand-field effects control the spin orientation.

Turning to the dinuclear DEB-bridged diradical systems, unrestricted B3LYP (UB3LYP) DFT was used to compute the lowest triplet and broken-symmetry M_S = 0 states for the cationic portions of **2** and **5** at their optimized geometries. The sum-rules approach of Ziegler, Rauk, and Baerends was used to estimate the triplet−singlet gap and hence the Heisenberg exchange coupling constant *J* (see eq 10):[56]

$$2J = \Delta E = E_{\alpha\alpha} - \frac{1}{2}(E_{\alpha\beta} + E_{\beta\alpha}) \qquad (10)$$

The final *J* parameters are presented in Table 2 along with experimental values; complete computational results for the dinuclear species are collected in Table S3 in the SI. For the para-substituted complex **2**, the computed *J* value is roughly half the magnitude of the observed value. For the meta-substituted complex **5**, *J* was computed to be nearly the same as the measured value and half as large as the value reported for the PF_6 salt analogue.[33] Empirically, pure density functionals tend to underestimate magnetic interactions, though inclusion of exact exchange in hybrid functionals such as B3LYP tends to reproduce magnetic behavior more precisely.[47]

For both the para- and meta-substituted complexes, the computed conformation maximizes the communication between the Fe^{III} centers (φ = 6 and 8°, respectively), whereas for the experimental structures, φ = 26° for para-substituted **2** and deviates significantly from φ = 0° for meta-bridged **5**.[75] It appears that the differences between the calculated and observed coupling values are largely the result of different orientational geometries.

To understand the magnetism of **4**, with the goal of generating increased interaction, a number of rotational and substitutional isomers were computationally investigated with d_{Fe-C} set to 1.873 Å; UB3LYP energies were computed for the individual quartet and $M_S = {}^1/_2$ microstates, and eqs 2−9 were used to estimate *J* as well as the Heisenberg energies (Table S4; see the SI for details). For the X-ray conformation of $[(dmpe)_6Cl_3Fe_3(TEB)]^{3+}$, two of the Fe interchelate dπ orbitals are nearly perpendicular to the aromatic π system. As discussed in the SI, two sets of low-lying quartet and $M_S = {}^1/_2$ microstates were found. The set consistent with experiment is summarized here. The computed *J* values are smaller than the observed ones, similar to the dinuclear calculations. Significantly, the pattern of computed *J* values (two small, one large) is consistent with experiment (see Table 2). The presence of one large *J* value is *not* consistent with a model that exclusively uses interchelate magnetic orbitals, as two of the interchelate dπ orbitals are oriented in the plane of the aromatic ring rather than being arranged perpendicular to it, yet a large *J* remains. Spin density plots for the quartet and individual $M_S = {}^1/_2$ microstates (Figure S17 in the SI) suggest that the same orbitals are spin-active for the quartet and the $M_S = {}^1/_2$ microstates. For all four single-determinant models, the spin density plots of the quartet and spin-flipped $M_S = {}^1/_2$ configurations (Figure 7 and Figure S17) reveal that one of the Fe centers utilizes an intrachelate dπ orbital to generate a significant Fe−Fe exchange interaction (Fe2). In effect, from a structural point of view, one "wrong" orbital is used for coupling. In addition, the magnetic orbital at Fe1 is canted out of the aryl π plane. The generality of this observation was confirmed by comparing computational results for four idealized orientational conformers: three singly-occupied magnetic orbitals parallel (PPP), two parallel and one perpendicular (PPA), one parallel and two perpendicular (PAA), and three perpendicular (AAA) to the central aryl π system. A schematic representation is presented in Figure 8; the data are collected in Table S5 in the SI, and the spin density plots are presented in Figures S18−S21 in the SI. The idealized PPP conformation with all three iron centers oriented to maximize the magnetic interactions does yield a substantially stabilized quartet state, three nearly equivalent *J* values, and equivalent spin density delocalization of each of the three $M_S = {}^1/_2$ microstates (Figure S18). Rotating one interchlelate magnetic orbital out of registry (PPA) does nearly quench two Fe−Fe interactions, substantially reducing the doublet−quartet gap (Figure S19) and leaving a single $M_S = {}^1/_2$ microstate (the one wherein the spin-flipped magnetic orbital is in the aryl plane) with significant α spin density

Table 2. Key Experimental and Computed Magnetostructural Parameters for Di- and Trinuclear Ethynylbenzene-Bridged Fe(III) Complexes

complex	E/C[a]	φ (deg)	J (cm^{-1})	ref
$[(dmpe)_4Fe_2Cl_2(\mu\text{-}p\text{-DEB})](BAr^F{}_4)_2$ (**2**)	E	28.1, 24.3	−134	*b*
$[(dmpe)_4Fe_2Cl_2(\mu\text{-}p\text{-DEB})]^{2+}$	C	3.9, 12.5	−83	*b*
$[(dppe)_2(Cp^*)_2Fe_2(\mu\text{-}p\text{-DEB})](PF_6)_2$	E	43.2	−191 (Paul)	25
	E		−1 (Lapinte)	18
$[(dHpe)_2(Cp)_2Fe_2(\mu\text{-}p\text{-DEB})]^{2+}$	C		−255	25
$[(dmpe)_6Fe_3Cl_3(\mu\text{-TEB})](OTf)_3$ (**4**)	E	36.9, 83.2, 83.2,	37, 5, 5	*b*
$[(dmpe)_6Fe_3Cl_3(\mu\text{-TEB})]^{3+}$ X-ray	C	37.4, 83.1, 83.5,	36, 2, 2	*b*
$[(dmpe)_6Fe_3Cl_3(\mu\text{-TEB})]^{3+}$ PPP[c]	C	1.3, 5.5, 14.5	49, 47, 47	*b*
$[(dmpe)_6Fe_3Cl_3(\mu\text{-TEB})]^{3+}$ PPA[c]	C	7.4, 12.9, 89.4	48, 2, 2	*b*
$[(dmpe)_6Fe_3Cl_3(\mu\text{-TEB})]^{3+}$ PAA[c]	C	5.5, 89.2, 87.6	51, 2, 2	*b*
$[(dmpe)_6Fe_3Cl_3(\mu\text{-TEB})]^{3+}$ AAA[c]	C	87.5, 88.6, 89.8	2, 2, −2	*b*
$[(dppe)_3(Cp^*)_3Fe_3(TEB)](PF_6)_3$	E	0.5, 53.6, 60.7	J = 9.6, J' = 4.4	19
$[(dppe)_3(Cp^*)_3Fe_3(TEB)]^{3+}$ X-ray[d]	C	0.7, 62.3, 62.3	34, 18, 9	*b*
$[(dppe)_3(Cp^*)_3Fe_3(TEB)]^{3+}$ PPP[c]	C	0.7, 1.5, 2.2	67, 67, 66	*b*
$[(dHpe)_3(Cp)_3Fe_3(TEB)]^{3+}$ PPP[c]	C	0.7, 1.5, 2.2	85, 83, 83	*b*
$[(dHpe)_3(Cp)_3Fe_3(TEB)]^{3+}$ PPP [e]	C	0.0, 4.1, 4.2	113, 111, 109	*b*
$[(dmpe)_4Fe_2Cl_2(\mu\text{-}m\text{-DEB})](BAr^F{}_4)_2$ (**5**)	E	∼21, 86 [f]	11	*b*
$[(dmpe)_4Fe_2Cl_2(\mu\text{-}m\text{-DEB})](PF_6)_2$	E	∼30, 80 [g]	41	33
$[(dmpe)_4Fe_2Cl_2(\mu\text{-}m\text{-DEB})]^{2+}$	C	5.3, 8.5	24	*b*
$[(dppe)_2(Cp^*)_2Fe_2(\mu\text{-}m\text{-DEB})](PF_6)_2$	E	61.7, 59.0	>150 (Paul)	25
	E		65.3 (Lapinte)	19
$[(dHpe)_2(Cp)_2Fe_2(\mu\text{-}m\text{-DEB})]^{2+}$	C	0, 4.5	256	25
$[(dppe)_2(Cp^*)_2Fe_2(\mu\text{-}m\text{-DEB})]^{2+}$	C	0.7, 1.5	36	*b*
$[(dHpe)_2(Cp)_2Fe_2(\mu\text{-}m\text{-DEB})]^{2+}$ X-ray[h]	C	0.7, 1.5	47	*b*
$[(dHpe)_2(Cp)_2Fe_2(\mu\text{-}m\text{-DEB})]^{2+}$ T[i]	C	0.4, 0.4	66	*b*
$[(dHpe)_2(Cp)_2Fe_2(\mu\text{-}m\text{-DEB})]^{2+}$ S[i]	C	0, 4.5	63	*b*

[a] E = experimental, C = computed. [b] This work. [c] Idealized structure: P = magnetic orbital parallel to the central aryl π system; A = magnetic orbital perpendicular to the π system. [d] These angles were measured from an idealized structure for the triferrous complex $[(dppe)_3(Cp^*)_3Fe_3(TEB)]$. [e] Geometry constructed on the basis of the X-ray structure of the dinuclear species in ref 25; approximate C_3 symmetry. [f] See ref 75. [g] A CIF file was not available for analysis, and the dmpe ligands are rotationally disordered in the structure. [h] The geometry was constructed from the X-ray structure in ref 23. [i] The geometry was constructed from the calculated triplet structure in ref 25.

delocalization (Figure S19d). This leads to a large $J_{Fe1,Fe2}$ and small $J_{Fe1,Fe2a}$ and $J_{Fe2,Fe2a}$. As discussed above for the X-ray-oriented calculations, rotating a second interchelate magnetic orbital out of registry (PAA) does not further reduce J, as again a state is found where one of the Fe centers, Fe2a, uses an intrachelate magnetic orbital to maintain the magnetic coupling (note the spin density plots in Figure S20, where Fe2a uses the structurally incorrect orbital). Rotation of all three sets of interchelate magnetic orbitals out of registry (AAA) nearly quenches the magnetic coupling; nevertheless, the spin density plots for this configuration (Figure S21) illustrate that a single dπ−aryl π interaction involving Fe2a can be maintained. Consistently, spin delocalization of at least one Fe-based magnetic orbital into the aryl π system can be operative in the $[(dmpe)_2FeCl]^{2+}$-based molecules, irrespective of the Fe−acetylide orbital orientation. From the standpoint of maximizing J, however, it is noted that the presence of even one perpendicularly oriented magnetic orbital gives rise to a low-energy doublet state, precluding robust isolation of high ground-state spins.

While the doublet−quartet gap for the orbitally aligned rotamer is significantly larger than that found for the X-ray conformation, it is substantially smaller than (computed or experimental) triplet−singlet gaps reported by Paul for the dinuclear Cp*-containing species (142 cm^{-1} for the geometry-optimized structure vs 23 cm^{-1} for the X-ray-determined orientation and 59 cm^{-1} as determined experimentally). Whereas ferromagnetic coupling in organic polyradicals is not perturbed by increased nuclearity,[10,60] others have observed weakened ferromagnetic coupling as the complex nuclearity increases;[76] if this were operative in the TEB-bridged system, elaboration to larger metallodendrimers would lead to a deleterious diminishment of the stabilization of high-spin ground states. To understand these differences, a model complex with the dmpe methyl substituents replaced by H atoms [i.e., using dHpe (more commonly denoted as dpe) rather than dmpe] was constructed. It should be noted that Paul and co-workers replaced phenyl groups with H atoms in their Cp* calculations.[25] Hydrogen substitution can impact the sterics of the model as well as the phosphine donor capacity. Gratifyingly, a near doubling of J as well as the doublet−quartet gap was computed (the energy gap increased from 142 to 220 cm^{-1}) without a significant change in geometry (Table S6 and Figure S22 in the SI). The lack of a geometry change suggests that H substitution does not sterically impact this system. Moreover, the increase in J suggests that hydrogen substitution does lead to better energy alignment between the Fe magnetic orbitals and the aromatic-bridge π^* orbitals, increasing the magnetic coupling.

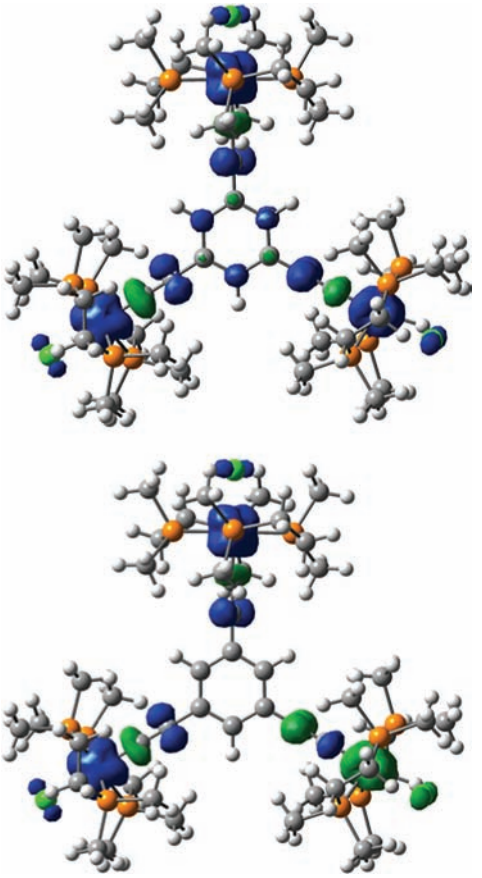

Figure 7. Illustrative spin density plots generated from UB3LYP calculations for the (top) $\alpha\alpha\alpha$ and (bottom) $\alpha\beta\alpha$ microstates of $[(dmpe)_6Cl_3Fe_3(TEB)]^{3+}$ based on the experimentally determined structure of **4**. All four spin density plots are provided in Figure S16 in the SI. Blue and green shading correspond to α and β spins, respectively; the 0.003 electron density |isovalue| surface is displayed. It should be noted that the lower-right iron uses an intrachelate magnetic orbital to maximize overlap with the aryl π system, whereas the other two Fe groups use interchelate magnetic orbitals.

To probe this hypothesis further, a series of substitutionally related model complexes were studied; the results are collected in Table S6 and Figure S23 in the SI. Replacing H with F or Cl again doubles J and the doublet−quartet gap. Substitution with OCH_3 yields only a modest increase relative to H. This computed trend correlates with the chelating phosphine HOMO orbital energy (Figure S24 in the SI), which serves as a measure of phosphine donor ability. The alternative MESP analysis[73] provided a reduced correlation due to the wide span in electronegativity of the phosphine substituents.[77,78] Notably, the HOMO analysis coupled with the orbital energy data in Table S7 in the SI suggests that J for dppe should be slightly larger than that for dmpe but significantly smaller than that for dHpe.

Two other computational studies were aimed to inform future dendrimer syntheses. First, to probe the impact of axial halide replacement on coupling, we found that substitution of Cl by either F or Br provides only a modest perturbation of J (Table S6 in the SI). Second, as an electronic effect, replacement of TEB^{3-} as the bridging ligand with the anionic form of 2,4,6-triethynylmesitylene (Me_3TEB^{3-}) causes only a modest perturbation of J. However, a more significant *geometric* stabilization is realized:

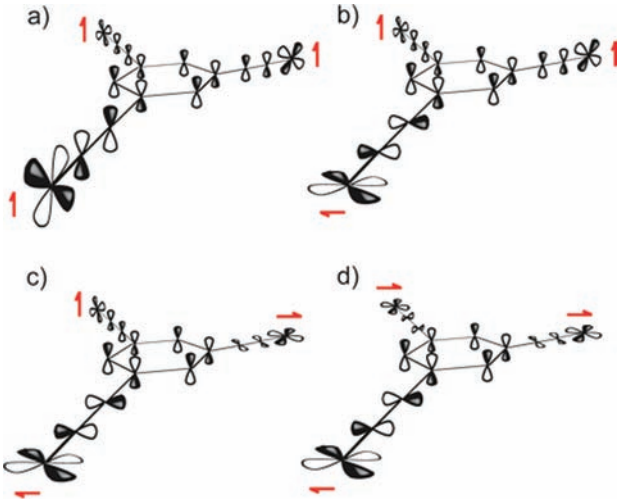

Figure 8. Idealized orientations of the "magnetic" dπ and acetylide pπ orbitals relative to the aryl π system in the cation of trinuclear **4**: (a) PPP; (b) PPA; (c) PAA; (d) AAA. Structurally, **4** would be expected to behave like (c), but its magnetism is most consistent with orbital arrangement (b).

the PPP structure, where all of the Fe^{III} magnetic orbitals are aligned with the aryl π system, was computed to be 5 kcal/mol more stable than the PPA rotamer, whereas for the parent complex $[(dmpe)_6Cl_3Fe_3(TEB)]^{3+}$, the PPP structure is stabilized by only 0.5 kcal/mol relative to the PPA rotamer.

Several computations were undertaken to investigate the impact of nuclearity on J (Figure S25 and Table S8 in the SI). First, $[(dHpe)_6Cl_3Fe_3(TEB)]^{3+}$ was reduced by one electron to give $[(dHpe)_6Cl_3Fe_3(TEB)]^{2+}$, leading to two magnetic orbitals and a singlet−triplet gap. Equation 10 was used to compute a J value of 59 cm^{-1}, slightly larger than but comparable to the *m*-DEB-bridged case studied above (48 cm^{-1}; Table S3 in the SI). In a second study, when one of the $[(dHpe)_2ClFe]^{2+}$ fragments was replaced by H, J was computed to drop to 44 cm^{-1}, almost identical to the *m*-DEB-bridged complex. For comparison, the average J value for $[(dHpe)_6Cl_3Fe_3(TEB)]^{3+}$ was calculated to be ~73 cm^{-1} (Table S6 in the SI). Computationally, an increase from two spin-active electrons to three does not appear to adversely affect J, suggesting that the assembly of higher-nuclearity species does not on its own lead to weaker exchange coupling.

To connect the present work to previously reported studies on Cp*-containing complexes,[18,24,25,63,65,71,79] unrestricted B3LYP energies were computed for the individual quartet and $M_S = {}^1/_2$ microstates for $[(dppe)_3Cp^*_3Fe_3(TEB)]^{3+}$. The computed J values are significantly larger than those observed experimentally (Table 2), although the computed values are based on symmetrized atomic coordinates from the Fe(II)-containing complex, since a structure of the Fe(III) analogue has not been reported. Strong pinning of the magnetic orbital identity by the Cp*(dppe) ligand set suggests that exchange interactions via bridge delocalization should be significantly enhanced by aligning the Fe magnetic orbitals with the aryl π system. For $[(dppe)_3Cp^*_3Fe_3(TEB)]^{3+}$, the orientational dependence of J was investigated by constructing a rotamer wherein the three magnetic orbitals were aligned with the aryl π system ($\varphi = 0°$; Figure S27 in the SI). J was computed to increase dramatically, from a minimum of 34 cm^{-1} to a maximum of 66 cm^{-1} (Table S9

in the SI). Since coupling for the Cp* system is so highly dependent on the relative Cp*(dppe)Fe orientation, it is likely that the as-isolated Fe^{III} complex features rotation of one or more $[(dppe)FeCp^*]^{2+}$ units further out of registry with the aryl π system.

Notably, the maximum J value for the spin-aligned species $[(dppe)_3Cp^*_3Fe_3(TEB)]^{3+}$ (66 cm^{-1}; Table S9 in the SI) is still appreciably smaller than that reported by Paul et al.[25] for $[(dHpe)_2Cp_2Fe_2(m\text{-DEB})]^{3+}$ (256 cm^{-1}). Several computational experiments were employed to probe this discrepancy; the results are summarized in Table 2, and details are provided in Tables S10 and S11 and Figures S26−S30 in the SI. From these computational studies, it was found that the same general trends apply to the Cp*/Cp-containing systems as to the $(dmpe)_2$-containing species presented here: first, the magnetic orbital orientation directly affects J; second, altering the ancillary ligand substituents modifies J but to a lesser extent than changing the magnetic orbital orientation. In addition, we found that regardless of the relative orientation of $[Cp^*(dppe)Fe]^{2+}$ units, triplets are more stable than singlets, with maximum J values in the 50−70 cm^{-1} range. There is no computational support either for large geometry changes upon magnetic excitation in these dinuclear complexes or for J to be as large as 250 cm^{-1}.

A final question to be addressed is the nature of the exchange pathway for the *m*-DEB- and TEB-bridged complexes. For *p*-DEB-bridged species, transmission of the cumulenic form across the bridge explains the strong AF exchange. For *m*-DEB- and TEB-bridged complexes, this valence-bond pathway is absent, and exchange/delocalization uses three fragment orbitals: the alkynyl π and π^* orbitals and the Fe-centered singly occupied magnetic orbital. Two hypotheses for exchange delocalization are the following: (1) direct delocalization from the singly occupied Fe dπ orbital into the alkynyl π^* orbital, leading to spin delocalization onto the aryl π system, and (2) donation from the doubly occupied alkynyl π orbital into the singly occupied Fe dπ orbital followed by a secondary back-donation from the singly occupied magnetic orbital (now Fe dπ−C pπ antibonding in character) into the alkynyl π^* orbital, leading to spin delocalization onto the aryl π system. The J−phosphine HOMO correlation investigation and a comparison of the spin natural orbitals for $[Cl(dmpe)_2Fe]^{2+}$ and $[Cl(dFpe)_2Fe]^{2+}$ support the latter hypothesis (Figure S31 in the SI). Regarding the J−phosphine HOMO correlation, decreased σ donation from the phosphine to the metal (via electron-withdrawing substituents) stabilizes the metal d orbital set by removing charge density from the metal center, leading to an increase in the interaction between the magnetic and aryl π system orbitals. If the interaction of the magnetic orbital with the aryl π^* system were the determining factor, electron-*donating* substituents would be expected to increase the J value, as this would destabilize the metal d orbital set and increase interaction with the aryl π^* system. The former trend was computationally observed for J. Visually, going from CH_3 to F, the set of nearly doubly occupied spin natural orbitals gain significant Fe dπ−C pπ bonding character and the set of nearly empty spin natural orbitals gain significant Fe dπ−C pπ antibonding character. The occupation numbers of the nearly filled orbitals decrease, while the nearly empty correlative orbitals gain electron density; this pattern is consistent with increased metal−ligand π bonding. The singly occupied magnetic orbitals display an increase in aryl π character. This model also provides an explanation for the increase in J as the nuclearity increases. In going from a dinuclear triplet to a trinuclear quartet system, a single favorable exchange interaction in the triplet is replaced by three favorable exchange interactions in the quartet. The arylalkynyl π^* system provides three orbitals (two e and one a) that can support three orthogonal delocalizations, each of which increases the magnetic exchange while lowering the energy of the system.

In summary, the computational studies provide evidence for strong orientational and phosphine donor strength dependencies of J and comparable exchange coupling parameters for $(dmpe)_2$ and (dppe)(Cp*) ligand frameworks as well as evidence against the suggestion that an increase in nuclearity leads to a decrease in magnetic coupling. In fact, at least for the system studied here, the opposite was found: for oriented rotamers, J was universally computed to increase by nearly a factor of 2 in going from two spins to three.

CONCLUSIONS AND OUTLOOK

The syntheses, structures, magnetic properties and results of electronic structure calculations for a series of Fe^{III} ethynylbenzene complexes have been described. Consistent with established topology rules, meta-bridged complexes **4** and **5** display $S = {}^3/_2$ and $S = 1$ ground states, respectively, at low temperatures, whereas para-bridged **2** shows antiferromagnetic interactions that lead to an $S = 0$ ground state. The relative strengths of the intramolecular exchange interactions are influenced by more subtle structural features. By means of DFT calculations, the orbital pathways responsible for the magnetic exchange interactions in Fe^{III} acetylide complexes have been determined and compared with those in Cp*-containing analogues. Whereas the Cp* complexes provide a robust structural handle connecting the relative geometry of ancillary ligand sets to the strength of intramolecular magnetic interactions, magnetic orbital control is more complex in the new complexes reported herein: the interplay between dπ/aromatic-π interactions, geometry, and ligand-field effects significantly impact the magnitude of the magnetic coupling. Nevertheless, the various factors can be deconvoluted for the Fe^{III} monomers and in principle applied to the understanding of higher-nuclearity species.

Importantly, substantial magnetic coupling strengths are foreseen for this class of complexes, provided that the magnetic orbitals can be tuned geometrically and electronically; the results of the preliminary computational exploration presented herein offer several synthetically accessible target molecules. The ability to manipulate J is expected to have profound implications for the preparation of low-dimensional metal complexes with well-isolated high-spin ground states, potentially resulting in molecular magnets with enhanced properties. Synthetic efforts to optimize the magnetic interactions in these and related complexes are underway.

ASSOCIATED CONTENT

Supporting Information. X-ray structural data for **1**, **2**, and **4** (CIF); details of computational work; complete ref 45; crystal data for **5**; spectral data; details of fitting procedures; computed data and spin density plots. This material is available free of charge via the Internet at http://pubs.acs.org.

AUTHOR INFORMATION

Corresponding Author
matthew.shores@colostate.edu

Present Addresses
[†]Pacific Northwest National Laboratory, Richland, WA 99352.

■ ACKNOWLEDGMENT

This research was supported by Colorado State University and ACS-PRF (44691-G3).

■ REFERENCES

(1) Long, N. J.; Williams, C. K. *Angew. Chem., Int. Ed.* **2003**, *42*, 2586.
(2) Ren, T. *Organometallics* **2005**, *24*, 4854.
(3) Sessoli, R.; Gatteschi, D.; Caneschi, A.; Novak, M. A. *Nature* **1993**, *365*, 141.
(4) *Single-Molecule Magnets and Related Phenomena*; Winpenny, R., Ed.; Structure and Bonding, Vol. 122; Springer: Berlin, 2006.
(5) Blagg, R. J.; Muryn, C. A.; McInnes, E. J. L.; Tuna, F.; Winpenny, R. E. P. *Angew. Chem., Int. Ed.* **2011**, *50*, 6530.
(6) Rinehart, J. D.; Fang, M.; Evans, W. J.; Long, J. R. *J. Am. Chem. Soc.* **2011**, *133*, 14236.
(7) Ruiz, E.; Rodríguez-Fortea, A.; Alvarez, S. *Inorg. Chem.* **2003**, *42*, 4881.
(8) Layfield, R. A.; McDouall, J. J. W.; Sulway, S. A.; Tuna, F.; Collison, D.; Winpenny, R. E. P. *Chem.—Eur. J.* **2010**, *16*, 4442.
(9) Jiang, S.-D.; Wang, B.-W.; Sun, H.-L.; Wang, Z.-M.; Gao, S. *J. Am. Chem. Soc.* **2011**, *133*, 4730.
(10) Rajca, A. *Chem. Rev.* **1994**, *94*, 871.
(11) Oshio, H.; Nakano, M. *Chem.—Eur. J.* **2005**, *11*, 5178.
(12) Cirera, J.; Ruiz, E.; Alvarez, S.; Neese, F.; Kortus, J. *Chem.—Eur. J.* **2009**, *15*, 4078.
(13) Tancini, E.; Rodriguez-Douton, M. J.; Sorace, L.; Barra, A.-L.; Sessoli, R.; Cornia, A. *Chem.—Eur. J.* **2010**, *16*, 10482.
(14) Onitsuka, K.; Fujimoto, M.; Kitajima, H.; Ohshiro, N.; Takei, F.; Takahashi, S. *Chem.—Eur. J.* **2004**, *10*, 6433.
(15) Onitsuka, K.; Fujimoto, M.; Ohshiro, N.; Takahashi, S. *Angew. Chem., Int. Ed.* **1999**, *38*, 689.
(16) McDonagh, A. M.; Humphrey, M. G.; Samoc, M.; Luther-Davies, B. *Organometallics* **1999**, *18*, 5195.
(17) McDonagh, A. M.; Powell, C. E.; Morrall, J. P.; Cifuentes, M. P.; Humphrey, M. G. *Organometallics* **2003**, *22*, 1402.
(18) Le Narvor, N.; Lapinte, C. *C. R. Acad. Sci., Ser. IIC: Chim.* **1998**, *1*, 745.
(19) Weyland, T.; Costuas, K.; Mari, A.; Halet, J.-F.; Lapinte, C. *Organometallics* **1998**, *17*, 5569.
(20) Packheiser, R.; Ecorchard, P.; Ruffer, T.; Lohan, M.; Brauer, B.; Justaud, F.; Lapinte, C.; Lang, H. *Organometallics* **2008**, *27*, 3444.
(21) Packheiser, R.; Lohan, M.; Brauer, B.; Justaud, F.; Lapinte, C.; Lang, H. *J. Organomet. Chem.* **2008**, *693*, 2898.
(22) Roué, S.; Le Stang, S.; Toupet, L.; Lapinte, C. *C. R. Chim.* **2003**, *6*, 353.
(23) Weyland, T.; Ledoux, I.; Brasselet, S.; Zyss, J.; Lapinte, C. *Organometallics* **2000**, *19*, 5235.
(24) Paul, F.; Lapinte, C. In *Unusual Structures and Physical Properties in Organometallic Chemistry*; Gielen, M., Willem, R., Wrackmeyer, B., Eds.; Wiley: Chichester, U.K., 2002.
(25) Paul, F.; Bondon, A.; da Costa, G.; Malvolti, F.; Sinbandhit, S.; Cador, O.; Costuas, K.; Toupet, L.; Boillot, M.-L. *Inorg. Chem.* **2009**, *48*, 10608.
(26) Paul, F.; Toupet, L.; Roisnel, T.; Hamon, P.; Lapinte, C. *C. R. Chim.* **2005**, *8*, 1174.
(27) Borden, W. T. *Mol. Cryst. Liq. Cryst.* **1993**, *232*, 195.
(28) Kheradmandan, S.; Venkatesan, K.; Blacque, O.; Schmalle, H. W.; Berke, H. *Chem.—Eur. J.* **2004**, *10*, 4872.
(29) Field, L. D.; George, A. V.; Hambley, T. W. *Inorg. Chem.* **1990**, *29*, 4565.
(30) Field, L. D.; George, A. V.; Laschi, F.; Malouf, E. Y.; Zanello, P. *J. Organomet. Chem.* **1992**, *435*, 347.
(31) We note that replacement of the axial chloride in these complexes is not facile. However, Field and co-workers have achieved stepwise ligand substitution starting with structurally analagous $[(dmpe)_2FeCH_3(C_2R)]$ complexes using photochemical methods. See ref 32.
(32) Field, L. D.; Turnbull, A. J.; Turner, P. *J. Am. Chem. Soc.* **2002**, *124*, 3692.
(33) Berben, L. A. Ph.D. Thesis, University of California, Berkeley, CA, 2005.
(34) Girolami, G. S.; Wilkinson, G.; Galas, A. M. R.; Thorntonpett, M.; Hursthouse, M. B. *J. Chem. Soc., Dalton Trans.* **1985**, 1339.
(35) Chávez, I.; Alvarez-Carena, A.; Molins, E.; Roig, A.; Maniukiewicz, W.; Arancibia, A.; Arancibia, V.; Brand, H.; Manríquez, J. M. *J. Organomet. Chem.* **2000**, *601*, 126.
(36) Connelly, N. G.; Geiger, W. E. *Chem. Rev.* **1996**, *96*, 877.
(37) Weber, E.; Hecker, M.; Koepp, E.; Orlia, W.; Czugler, M.; Csöregh, I. *J. Chem. Soc., Perkin. Trans. 2* **1988**, 1251.
(38) *APEX 2*; Bruker Analytical X-Ray Systems, Inc.: Madison, WI, 2009.
(39) Sheldrick, G. M. *SHELXTL*; Bruker Analytical X-Ray Systems, Inc.: Madison, WI, 1999.
(40) Spek, A. L. *PLATON: A Multipurpose Crystallographic Tool*; Utrecht University: Utrecht, The Netherlands, 2005.
(41) Kahn, O. *Molecular Magnetism*; VCH: New York, 1993.
(42) Bill, E. *julX*, version 1.41; Max Planck Institute for Bioinorganic Chemistry: Mulheim an der Ruhr, Germany, 2008; http://www.mpibac.mpg.de/bac/logins/bill/julX_en.php. (accessed July 26, 2011).
(43) Schmitt, E. A. Ph.D. Thesis, University of Illinois at Urbana-Champaign, Urbana, IL, 1995.
(44) Becke, A. D. *J. Chem. Phys.* **1993**, *98*, 5648.
(45) Frisch, M. J.; et al. *Gaussian 09*; Gaussian, Inc.: Wallingford, CT, 2009.
(46) Bacskay, G. B. *Chem. Phys.* **1981**, *61*, 385.
(47) Seeger, R.; Pople, J. A. *J. Chem. Phys.* **1977**, *66*, 3045.
(48) Hay, P. J.; Wadt, W. R. *J. Chem. Phys.* **1985**, *82*, 299.
(49) Ditchfield, R.; Hehre, W. J.; Pople, J. A. *J. Chem. Phys.* **1971**, *54*, 724.
(50) Hehre, W. J.; Ditchfield, R.; Pople, J. A. *J. Chem. Phys.* **1972**, *56*, 2257.
(51) Binkley, J. S.; Pople, J. A.; Hehre, W. J. *J. Am. Chem. Soc.* **1980**, *102*, 939.
(52) Francl, M. M.; Pietro, W. J.; Hehre, W. J.; Binkley, J. S.; Gordon, M. S.; DeFrees, D. J.; Pople, J. A. *J. Chem. Phys.* **1982**, *77*, 3654.
(53) Weyland, T.; Lapinte, C.; Frapper, G.; Calhorda, M. J.; Halet, J.-F.; Toupet, L. *Organometallics* **1997**, *16*, 2024.
(54) Noodleman, L.; Davidson, E. R. *Chem. Phys.* **1986**, *109*, 131.
(55) Soda, T.; Kitagawa, Y.; Onishi, T.; Takano, Y.; Shigeta, Y.; Nagao, H.; Yoshioka, Y.; Yamaguchi, K. *Chem. Phys. Lett.* **2000**, *319*, 223.
(56) Ziegler, T.; Rauk, A.; Baerends, E. J. *Theor. Chim. Acta* **1977**, *43*, 261.
(57) Slipchenko, L. V.; Krylov, A. I. *J. Chem. Phys.* **2003**, *118*, 9614.
(58) Wang, F.; Ziegler, T. *J. Chem. Phys.* **2004**, *121*, 12191.
(59) Rinkevicius, Z.; Agren, H. *Chem. Phys. Lett.* **2010**, *491*, 132.
(60) Borden, W. T.; Iwamura, H.; Berson, J. A. *Acc. Chem. Res.* **1994**, *27*, 109.
(61) Ishida, T.; Iwamura, H. *J. Am. Chem. Soc.* **1991**, *113*, 4238.
(62) Kanno, F.; Inoue, K.; Koga, N.; Iwamura, H. *J. Phys. Chem.* **1993**, *97*, 13267.
(63) Le Narvor, N.; Lapinte, C. *Organometallics* **1995**, *14*, 634.
(64) de Montigny, F.; Argouarch, G.; Costuas, K.; Halet, J.-F.; Roisnel, T.; Toupet, L.; Lapinte, C. *Organometallics* **2005**, *24*, 4558.
(65) Weyland, T.; Costuas, K.; Mari, A.; Halet, J. F.; Lapinte, C. *Organometallics* **1998**, *17*, 5569.
(66) Stoll, S.; Schweiger, A. *J. Magn. Reson.* **2006**, *178*, 42.
(67) Rinehart, J. D.; Harris, T. D.; Kozimor, S. A.; Bartlett, B. M.; Long, J. R. *Inorg. Chem.* **2009**, *48*, 3382.
(68) Newell, B. S.; Rappé, A. K.; Shores, M. P. *Inorg. Chem.* **2010**, *49*, 1595.

(69) Lescouĕzec, R.; Lloret, F.; Julve, M.; Vaissermann, J.; Verdaguer, M. *Inorg. Chem.* **2002**, *41*, 818.
(70) Colacio, E.; Ghazi, M.; Stoeckli-Evans, H.; Lloret, F.; Moreno, J. M.; Pérez, C. *Inorg. Chem.* **2001**, *40*, 4876.
(71) Tanaka, Y.; Shaw-Taberlet, J. A.; Justaud, F.; Cador, O.; Roisnel, T.; Akita, M.; Hamon, J.-R.; Lapinte, C. *Organometallics* **2009**, *28*, 4656.
(72) Cowley, R. E.; DeYonker, N. J.; Eckert, N. A.; Cundari, T. R.; DeBeer, S.; Bill, E.; Ottenwaelder, X.; Flaschenriem, C.; Holland, P. L. *Inorg. Chem.* **2010**, *49*, 6172.
(73) Bonniard, L.; Kahlal, S.; Diallo, A. K.; Ornelas, C.; Roisnel, T.; Manca, G.; Rodrigues, J.; Ruiz, J.; Astruc, D.; Saillard, J.-Y. *Inorg. Chem.* **2011**, *50*, 114.
(74) Borden, W. T.; Davidson, E. R. *J. Am. Chem. Soc.* **1977**, *99*, 4587.
(75) On the basis of our structural data for **5**, $\varphi = 21°$ and 86°, but the presence of dmpe rotational disorder preventd an accurate determination. Similar disorder was observed by Berben for the PF_6 analogue of **5**.
(76) Shores, M. P.; Sokol, J. J.; Long, J. R. *J. Am. Chem. Soc.* **2002**, *124*, 2279.
(77) Kühl, O. *Coord. Chem. Rev.* **2005**, *249*, 693.
(78) Giering, W. P.; Prock, A.; Fernandez, A. L. *Inorg. Chem.* **2003**, *42*, 8033.
(79) Le Narvor, N.; Toupet, L.; Lapinte, C. *J. Am. Chem. Soc.* **1995**, *117*, 7129.